



Line Lists for the $X^1\Sigma^+$ State of CS

Shilin Hou and Zhengxing Wei

Department of Physics, Ocean University of China, Qingdao, Shandong 266100, People's Republic of China; slhou@ouc.edu.cn

Received 2019 November 5; revised 2019 December 6; accepted 2019 December 6; published 2020 January 16

Abstract

Rotation-vibrational line lists for eight isotopologues of carbon monosulphide (CS; $^{12}\text{C}^{32}\text{S}$, $^{12}\text{C}^{33}\text{S}$, $^{12}\text{C}^{34}\text{S}$, $^{12}\text{C}^{36}\text{S}$, $^{13}\text{C}^{32}\text{S}$, $^{13}\text{C}^{33}\text{S}$, $^{13}\text{C}^{34}\text{S}$, and $^{13}\text{C}^{36}\text{S}$) in their ground electronic state ($X^1\Sigma^+$) are calculated. An empirical potential function with the corrections of Born–Oppenheimer breakdown effects, which are determined by a direct potential fitting approach using over 4300 observed transition frequencies of $^{12}\text{C}^{32}\text{S}$, $^{12}\text{C}^{33}\text{S}$, $^{12}\text{C}^{34}\text{S}$, and $^{13}\text{C}^{32}\text{S}$, is used in line list calculations. The reproduced transition frequencies are within the observation uncertainties for the isotopologues with experimental data. The dipole moment functions are calculated using an ab initio method at a multireference configuration interaction method/cc-pv5z level with a large active space of electronic configuration. The dipole moment at equilibrium nuclear separation is almost identical to the experimental result. The calculated intensities agree excellently with the laboratory observations at 2573 K. The corresponding Einstein A coefficients and oscillator strengths are predicted. Partition functions for temperatures up to 7500 K have been calculated. The line lists can be used for spectroscopic measurements of CS in astronomical environments of various temperatures.

Unified Astronomy Thesaurus concepts: [Spectral line lists \(2082\)](#)

Supporting material: FITS file, machine-readable tables

1. Introduction

Carbon monosulphide (CS), similar to CO, H_2CO , etc., is one of the most important interstellar species of great astrophysical interest (Paulose et al. 2015; Heays et al. 2017; Maxted et al. 2018; McGuire 2018; Riaz et al. 2019). After the detection by Penzias et al. (1971) of the $J = 3 \rightarrow 2$ transition of CS at 146,969 MHz toward Orion, W51, IRC+10216, and DR21, CS was the first confirmed sulfur-containing species in the interstellar medium (ISM). Since then, CS has been observed in various ISM or objects, such as comets (Woodney et al. 1997; Canaves et al. 2007) and the atmosphere of Jupiter in the solar system (Moreno et al. 2003), star-forming regions (Heikkila et al. 1999; Rubio et al. 2009; Indebetouw et al. 2013), protostellar envelopes (Herpin et al. 2012), dense interstellar clouds (Hasegawa et al. 1984; Hayashi et al. 1985; Destree et al. 2009), planetary nebulae (Edwards & Ziurys 2014), carbon-rich stars (Ridgway et al. 1977; Tenenbaum et al. 2010), oxygen-rich stars (Ziurys et al. 2007; Tenenbaum et al. 2010; Danilovich et al. 2019), supernova remnants (Maxted et al. 2018), proto-brown dwarfs (Riaz et al. 2019), and so on.

Quantitative laboratory data are required to simulate the spectral energy distributions of astronomical objects (Bernath 2014). High-resolution laboratory spectra of CS have extensively been studied in various wavelength regions from microwave (MW) to ultraviolet. Reliable line lists to calculate molecular opacities can be obtained through a combination of laboratory data and ab initio calculations.

The laboratory MW spectrum of CS was first reported by Mockler & Bird (1955). The rotational transitions in the vibrational excited states up to $v = 20$, 7, and 3 were observed by Bogey et al. (1982) for $^{12}\text{C}^{32}\text{S}$, $^{12}\text{C}^{34}\text{S}$, and $^{13}\text{C}^{33}\text{S}$, respectively. Transitions of J up to $J = 23-22$ were reported by Ahrens & Winniewisser (1999) for various isotopic species in vibrational states of $v = 0-16$ ($^{12}\text{C}^{32}\text{S}$), $0-2$ ($^{12}\text{C}^{33}\text{S}$), $0-8$ ($^{12}\text{C}^{34}\text{S}$), $0-1$ ($^{12}\text{C}^{36}\text{S}$), $0-5$ ($^{13}\text{C}^{32}\text{S}$), 0 ($^{13}\text{C}^{33}\text{S}$), and $0-2$ ($^{13}\text{C}^{34}\text{S}$). Later, Kim & Yamamoto (2003) observed the $J = 1-0$ transitions in vibrational states up to $v = 39$, 16, 7, and 9 for $^{12}\text{C}^{32}\text{S}$, $^{12}\text{C}^{34}\text{S}$, $^{12}\text{C}^{33}\text{S}$, and $^{13}\text{C}^{32}\text{S}$,

respectively. The $J = 2-1$ transitions of $v = 18-22$ were also observed for $^{12}\text{C}^{32}\text{S}$ (Aoki et al. 1998).

High-resolution infrared (IR) measurements of the $1-0$ and $2-1$ bands of $^{12}\text{C}^{32}\text{S}$ and $1-0$ bands of $^{12}\text{C}^{33}\text{S}$, $^{12}\text{C}^{34}\text{S}$, and $^{13}\text{C}^{32}\text{S}$ were reported by Burkholder et al. (1987). The rotational levels were up to $J_{\text{max}} = 41$, 28, 32, and 28 for $^{12}\text{C}^{32}\text{S}$, $^{12}\text{C}^{33}\text{S}$, $^{12}\text{C}^{34}\text{S}$, and $^{13}\text{C}^{32}\text{S}$, respectively. The accuracy of the Burkholder et al. (1987) data was expected to be $\pm 0.00022 \text{ cm}^{-1}$. Later, Ram et al. (1995) obtained the transitions of $^{12}\text{C}^{32}\text{S}$ for bands of $\Delta v = 1$, $v = 0-9$ at 2573 K. The highest rotational levels were assigned to $J_{\text{max}} = 115$, with precisions of high-quality measurements (for $v \leq 5$) up to $\pm 0.0005 \text{ cm}^{-1}$; for bands of $v > 5$, the estimated precision was about $\pm 0.002 \text{ cm}^{-1}$. Recently, Uehara et al. (2015) obtained the $\Delta v = 1$ vibrational-rotational spectra of $^{13}\text{C}^{32}\text{S}$ and $^{12}\text{C}^{32}\text{S}$ for bands up to $v = 5-4$ and $7-6$, respectively. The uncertainties for the measurements of bands $v = 1-0$ to $5-4$ of $^{13}\text{C}^{32}\text{S}$ and $v = 1-0$ to $6-5$ of $^{12}\text{C}^{32}\text{S}$ were estimated to be $\pm 0.0003 \text{ cm}^{-1}$; those for band $v = 7-6$ of $^{12}\text{C}^{32}\text{S}$ were $\pm 0.0015 \text{ cm}^{-1}$.

The IR $\Delta v = 2$ bands were observed in the stellar envelope of TX Psc by the *Infrared Space Observatory* SWS spectrometer (Aoki et al. 1998), where the six band heads of $v = 2-0$ to $7-5$ were assigned. Laboratory spectroscopic studies of the $\Delta v = 2$ bands were reported by Todd (1977) and later Winkel et al. (1984), who analyzed seven bands from $v = 2-0$ to $8-6$. In a very recent paper, the $\Delta v = 2$ overtone bands of $^{12}\text{C}^{32}\text{S}$ were reported up to $v = 28-26$ and J_{max} up to 24 in the $1890-2580 \text{ cm}^{-1}$ region (Kawaguchi & Deo 2019). The spectra were recorded with the Bruker IFS 120 HR spectrometer by using a 0.03 cm^{-1} resolution.

For transitions involving the ground electronic state of CS, spectra have been recorded and analyzed by a variety of researchers. The $A^1\Pi-X^1\Sigma^+$ emission was first photographed by Crawford & Shurcliff (1934). The emission band of $A^1\Pi-X^1\Sigma^+$ was recorded, and the radiative lifetimes of different vibrational states of $A^1\Pi$ were measured (Smith 1969; Carlson et al. 1979; Hynes & Brophy 1979; Mahon et al. 1997). The spin-forbidden transition $a^3\Pi-X^1\Sigma^+$ of CS was also

observed at high resolution in the near-ultraviolet region (Cossart et al. 1977; Fournier et al. 1979). The $B^1\Sigma^+-X^1\Sigma^+$ (Donovan et al. 1970) and $C^1\Sigma^+-X^1\Sigma^+$ (Stark et al. 1987) transitions have been recorded and assigned by analogy with the valence isoelectronic species CO, which suggests that the B state of CS has a Rydberg nature like the corresponding state of CO. Stark et al. (1987) also found additional vibrational components of the B–X transition; the obtained spectroscopic constants of the B state are close to those of the CS^+ ground state, which strongly supports the proposed Rydberg nature of the B state. Based on the reliable spectral data of the low-lying states, more difficult analyses may become possible for complicated transitions involving strong perturbations (Li et al. 2013a).

Ab initio studies on CS have recently been extensively performed using the internally contracted multireference configuration interaction (MRCI) method. Pattillo et al. (2018) calculated the photodissociation cross sections from the $X^1\Sigma^+$ state to six low-lying excited electronic states ($A^1\Sigma^+$, $A^1\Pi$, $2^1\Pi$, $3^1\Pi$, $B^1\Sigma^+$, and $4^1\Pi$) for temperatures ranging from 1000 to 10,000 K using the MRCI approach with the Davidson correction (MRCI+Q). Fourteen molecular orbitals (MOs), which can be expressed with $(8a_1, 3b_1, 3b_2, 0a_2)$ using the irreducible representations of the C_{2v} point group, were used to perform the related calculations with the aug-cc-pv6z (av6z) basis sets. Shi et al. (2011) computed the potential curves for several low-lying electronic states ($X^1\Sigma^+$, $a^3\Pi$, $a'^3\Sigma^+$, $d^3\Delta$, $e^3\Sigma^-$, and $A^1\Pi$) with methods and basis sets that were the same as or similar to those of Pattillo et al. (2018). Besides the states investigated by Shi et al. (2011), Li et al. (2013b) studied additional low-lying states ($1^1\Sigma^-$, $1^1\Delta$, $1^5\Pi$, $A^1\Sigma^+$, $2^3\Pi$, and $1^5\Sigma^+$) with the MRCI+Q approach, including spin–orbit coupling, using the aug-cc-pwCV5Z basis sets. The active spaces of Shi et al. (2011) and Li et al. (2013b) are also the same as those of Pattillo et al. (2018). In their works, molecular potentials and transitional dipole moments between some electronic states were calculated. However, the related permanent dipole moment function for a given electronic state (e.g., $X^1\Sigma^+$) was not available in the literature mentioned above. Ornellas (1998) investigated the transition moment function, transition probabilities, and radiative lifetimes in the $A^1\Pi-X^1\Sigma^+$ system of the CS molecule using MRCI theory with MOs from $(8a_1, 3b_1, 3b_2, 0a_2)$ to $(9a_1, 4b_1, 4b_2, 1a_2)$ and basis sets of cc-pvxx ($x = t, q, 5$). Permanent dipole moments for both the X and A states were also available in Ornellas (1998). For the X state, there were at least two points (in the range of 2.2–10.0 Bohr) with dipole moments of zero. This is different from many of the other general species in their ground states. In addition, we noticed that the details of the dipole moments of the ground state in the ranges of $R < 2.2$ and $5.0 < R < 6.5$ Bohr were not available, which might also be important for predictions of accurate intensities for transitions involving the states of high vibration-rotational excited levels.

The most recent empirical potential function of CS determined by fitting observed transition frequencies was obtained by Coxon & Hajigeorgiou (1992). Such a potential function can reproduce spectra with the observation accuracies. With the potential of Coxon & Hajigeorgiou (1992) and the analytic dipole moment function of Pineiro et al. (1987), the line lists for the CS ground state were calculated by Paulose et al. (2015). In their work, numerical turning points of the Coxon & Hajigeorgiou (1992)

potential in the range of $R = 1.0\text{--}3.0$ Å were used. To avoid nonphysical intensity anomalies caused by numerical functions (Medvedev et al. 2016, 2017), the overtone transitions were predicted up to $\Delta v = 9$ for $v = 0\text{--}49$ and J_{\max} up to 258. Their line lists span frequencies of up to $11,000\text{ cm}^{-1}$. The simulated intensities of predicted lines, unfortunately, were overlarge for the strongest lines in the predicted spectrum.

As is known, the quality of the molecular potential function from fitting is related to both the qualities and the quantities of the observed data. At present, to the best of our knowledge, an accurate molecular potential function from accurate spectral data after 1992 is not available for the ground state of CS. In addition, a high-quality ab initio dipole moment function for the $X^1\Sigma^+$ state is also needed to obtain satisfactory intensities for a wide range of transition frequencies relative to high rovibrational levels of CS, which are of great importance for studies of the objects in various astronomical environments.

In the present work, line lists for eight isotopologues of CS ($^{12}C^{32}S$, $^{12}C^{33}S$, $^{12}C^{34}S$, $^{12}C^{36}S$, $^{13}C^{32}S$, $^{13}C^{33}S$, $^{13}C^{34}S$, and $^{13}C^{36}S$) are calculated using an empirical potential function including Born–Oppenheimer approximation breakdown (BOB) corrections, which are obtained through fitting with the latest observed frequencies in the range of $v = 0\text{--}28$, and J_{\max} up to 114. Permanent dipole moment functions are calculated and optimized with high-level ab initio methods. Transition intensities predicted with refined dipole moment functions from high-level MRCI/cc-pv5z calculations are in excellent agreement with the observed spectrum. The final line lists are produced for overtone transitions within $15,000\text{ cm}^{-1}$, which cover most of the transitions of $\Delta v \leq 12$ for $v = 0\text{--}59$ and J_{\max} up to 260.

2. Methods and Results

The empirical molecular potential function is obtained using a direct potential fitting (DPF) approach (LeRoy 2017a) based upon over 4300 observed transition frequencies of $^{12}C^{32}S$, $^{12}C^{33}S$, $^{12}C^{34}S$, and $^{13}C^{32}S$; dipole moment functions are calculated with high-level ab initio approaches. Line lists for eight isotopologues of CS are obtained with LEVEL (LeRoy 2017b) using the DPF potential and refined analytic dipole moment functions.

2.1. Potential Energy Function

The molecular potential is obtained by fitting with an effective radial Schrödinger equation (Watson 1980; LeRoy & Huang 2002), in which the BOB effects are accounted for by incorporation of atomic mass–dependent correction functions in the electronic and centrifugal parts of the effective potential energy function. For isotopologue α of the molecule, this equation can be written as (Watson 1980; LeRoy & Huang 2002)

$$\left\{ -\frac{\hbar^2}{2\mu_\alpha} \frac{d^2}{dr^2} + [V_{\text{ad}}(r) + \Delta V_{\text{ad}}^{(\alpha)}(r)] + \frac{\hbar^2 J(J+1)}{2\mu_\alpha r^2} [1 + q^{(\alpha)}(r)] - E_{v,J}(r) \right\} \Psi_{v,J}(r) = 0, \quad (1)$$

where μ_α is the reduced mass, $V_{\text{ad}}(r)$ is the total effective internuclear potential for the reference species ($^{12}C^{32}S$ in this work), and $\Delta V_{\text{ad}}^{(\alpha)}(r)$ and $q^{(\alpha)}(r)$ are the adiabatic BOB radial

Table 1
Laboratory Data Used in EMO Potential Fitting

	Transitions ^a	Frequency (cm ⁻¹)	No. of Lines	References
¹² C ³² S	$\nu = 0-10, J \leq 23; \nu = 11-16, J \leq 7; \nu = 17-20, J \leq 3; \nu = 21-26, J = 1 (\Delta\nu = 0)$	1.3–36	155	1, 2, 3, 4
¹² C ³³ S	$\nu = 0-2; J \leq 22 (\Delta\nu = 0)$	9.6–35.6	16	1
¹² C ³⁴ S	$\nu = 0-9; J \leq 22 (\Delta\nu = 0)$	1.5–35.4	70	1, 3
¹³ C ³² S	$\nu = 0-5; J \leq 23 (\Delta\nu = 0)$	1.5–35.5	48	1, 3
¹² C ³² S	$\nu = 0-9; J \leq 114 (\Delta\nu = 1)$	1036–1373	1587	5, 6, 7
¹² C ³³ S	$\nu = 0-1; J \leq 29 (\Delta\nu = 1)$	1221–1309	54	5
¹² C ³⁴ S	$\nu = 0-1; J \leq 36 (\Delta\nu = 1)$	1197–1311	70	5
¹³ C ³² S	$\nu = 0-5; J \leq 86 (\Delta\nu = 1)$	1080–1326	626	5, 8
¹² C ³² S	$\nu = 0-2; J \leq 111 (\Delta\nu = 2)$	2318–2559	189	7
¹² C ³² S	$\nu = 0-28; J \leq 37 (\Delta\nu = 2)$	1861–2559	1581	9
Sum	4396	...

Note.

^a All transitions satisfy the dipole selection rule $\Delta J = \pm 1$.

References. (1) Ahrens & Winniewisser (1999), (2) Aoki et al. (1998), (3) Bogey et al. (1982), (4) Kim & Yamamoto (2003), (5) Burkholder et al. (1987), (6) Ram et al. (1995), (7) Winkel et al. (1984), (8) Uehara et al. (2015), (9) Kawaguchi & Deo (2019).

potential correction and the nonadiabatic centrifugal potential correction function for isotopologue α , respectively.

The total effective internuclear potential, $V_{\text{ad}}(r)$, takes the model of the expanded Morse oscillator (EMO; LeRoy 2017a), which has a formulism as follows:

$$V_{\text{EMO}}(r) = D_e [1 - e^{-\phi(r)(r-r_e)}]^2, \quad (2)$$

$$\phi(r) = \sum_{i=0}^N \beta_i [y_p(r)]^i. \quad (3)$$

The adiabatic BOB functions, $\Delta V_{\text{ad}}^{(\alpha)}(r)$, are scaled by $\Delta M(\alpha)/M(\alpha)$ and expanded as

$$\Delta V_{\text{ad}}^{(\alpha)}(r) = \frac{\Delta M_C^{(\alpha)}}{M_C^{(\alpha)}} \Delta V_{\text{ad}}^C(r) + \frac{\Delta M_S^{(\alpha)}}{M_S^{(\alpha)}} \Delta V_{\text{ad}}^S(r), \quad (4)$$

where

$$\Delta M_X(\alpha) = M_X(\alpha) - M_X(^{12}\text{C} \text{ or } ^{32}\text{S}), \quad (5)$$

$$\Delta V_{\text{ad}}^X(r) = [1 - y_m(r)] \sum_{i=1} u_i^X [y_p(r)]^i, \quad (6)$$

for $X = \text{C}$ and S .

The nonadiabatic centrifugal BOB functions are expanded as

$$q^{(\alpha)}(r) = \frac{M(^{12}\text{C})}{M_C^{(\alpha)}} q_C(r) + \frac{M(^{32}\text{S})}{M_S^{(\alpha)}} q_S(r), \quad (7)$$

where

$$q_X(r) = \left[1 - y_p(r) \right] \sum_{i=1}^i t_i^X [y_{q_{\text{NA}}}(r)]^i, \quad (8)$$

$$y_K(r) = (r^K - r_e^K) / (r^K + r_e^K), \quad (9)$$

for $K = m, p$, and q_{NA} and $X = \text{C}$ and S , respectively. Integer parameters are set to $N = 7$ and $p = 3$ in Equation (3), $m = 3$ in Equation (6), and $q_{\text{NA}} = 2$ in Equation (8).

The dissociation energy D_e takes $59,947 \text{ cm}^{-1}$, which is obtained using $D_e = D_0 + E(0)$. Here $D_0 = 7.353$ (25) eV is taken from Coppens & Drowart (1995); $E(0)$, the zero-point energy (ZPE) of ¹²C³²S (641.03 cm^{-1}), is from Uehara et al. (2015). Several different values for D_e in the range of

Table 2

Fitted Parameters of the Empirical EMO Function for the $X^1\Sigma^+$ State of CS^a

	$V_{\text{EMO}} (N = 7, p = m = 3, q_{\text{NA}} = 2)$	Uncertainty
D_e (cm ⁻¹)	59,947	Fixed
r_e (Å)	$1.534942478421 \times 10^0$	2.1×10^{-7}
β_0 (Å ⁻¹)	$1.888128012269 \times 10^0$	3.0×10^{-7}
β_1 (Å ⁻¹)	$8.466123605894 \times 10^{-3}$	6.7×10^{-5}
β_2 (Å ⁻¹)	$1.178173273877 \times 10^{-1}$	1.0×10^{-4}
β_3 (Å ⁻¹)	$9.300138823638 \times 10^{-2}$	4.3×10^{-4}
β_4 (Å ⁻¹)	$1.551103858002 \times 10^{-1}$	9.3×10^{-4}
β_5 (Å ⁻¹)	$1.404488741192 \times 10^{-1}$	5.7×10^{-3}
β_6 (Å ⁻¹)	$6.642614487879 \times 10^{-2}$	1.7×10^{-2}
β_7 (Å ⁻¹)	$4.356680194779 \times 10^{-1}$	1.6×10^{-2}
u_1^C (cm ⁻¹)	$3.601618727588 \times 10^1$	1.9×10^0
u_2^C (cm ⁻¹)	$-7.176120636785 \times 10^1$	3.0×10^0
u_3^C (cm ⁻¹)	$4.149433529935 \times 10^1$	9.5×10^0
u_1^S (cm ⁻¹)	$1.303777937842 \times 10^1$	2.2×10^0
u_2^S (cm ⁻¹)	$-1.528554372158 \times 10^1$	3.6×10^0
t_1^C (cm ⁻¹)	$-1.174611607216 \times 10^{-4}$	3.1×10^{-5}
t_2^C (cm ⁻¹)	$-1.105246915417 \times 10^{-3}$	3.0×10^{-4}

Notes. The input file for LEVEL8.0, which contains all the data in this table, is given as supplementary data.

^a Using ¹²C³²S as a reference.

(This table is available in its entirety in FITS format.)

$59,300-60,500 \text{ cm}^{-1}$ are tried; however, the influence of D_e is not significant on the predicted transitions in the range of the observed frequencies.

The observed transition frequencies of ¹²C³²S, ¹²C³³S, ¹²C³⁴S, and ¹³C³²S are used in a least-squares fit to determine the effective Hamiltonian specified in Equation (1). Fitting is performed with Dpotfit (LeRoy 2017a), based upon 4396 transitions in total, including the rovibrational transitions of $\Delta\nu = 1$ for $\nu = 0-9$, J up to 114, overtone transitions of $\Delta\nu = 2$ for $\nu = 0-28$, and pure rotational transitions of ν up to 26. The details of the observed data used in the fit are listed in Table 1. The final obtained empirical EMO potential parameters are given in Table 2. The input file to LEVEL that contains all of the information on the present EMO potential function is also provided as supplementary data.

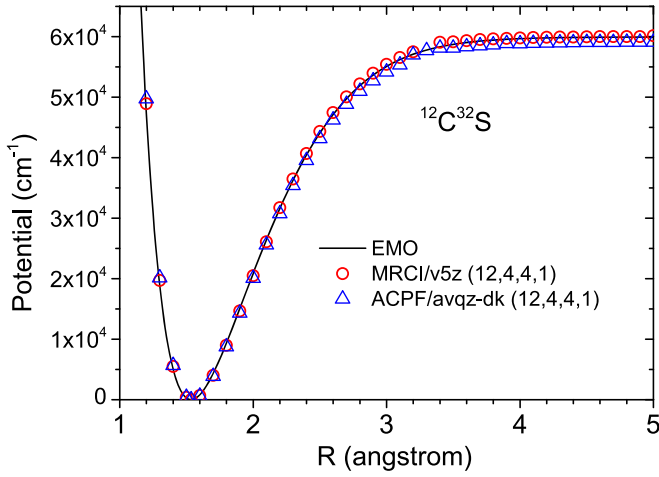


Figure 1. Fitted EMO function and calculated ab initio potentials. The EMO potential (solid line) is obtained by fitting the observed transitions listed in Table 1 with Dpotfit (LeRoy 2017b); MRCI (circles) and ACPF (triangles) data are obtained with the MOLPRO package. Computational details are given in Section 2.2 in text. For comparison, ab initio data are shifted to zero at R_e .

Figure 1 compares the EMO potential with high-level ab initio data to insure safe long-range behavior. Ab initio potentials are obtained with MRCI and averaged coupled-pair functional (ACPF) approaches using a large active space of electronic configuration. Figure 1 demonstrates that the EMO potential is in good agreement with the high-quality MRCI data (computational details are given in Section 2.2).

The quality of the obtained EMO potential can be indicated with deviations to the observed transition frequencies, which are plotted in Figure 2. The results for $^{12}\text{C}^{32}\text{S}$ and $^{13}\text{C}^{32}\text{S}$ are shown in Figures 2(a) and (b), respectively. For most of the calculated transitions, the deviations are within 0.003 and 0.002 cm^{-1} for $^{12}\text{C}^{32}\text{S}$ and $^{13}\text{C}^{32}\text{S}$, respectively. Figure 2(c) gives the comparison for $\Delta\nu = 2$ overtone transitions of $^{12}\text{C}^{32}\text{S}$; the corresponding differences from the observed data are within 0.01 cm^{-1} for most of the predictions. Figure 2(d) presents comparisons between observed and calculated transitions for $^{12}\text{C}^{33}\text{S}$ (squares), $^{12}\text{C}^{34}\text{S}$ (circles), $^{12}\text{C}^{36}\text{S}$ (upward triangles), $^{13}\text{C}^{33}\text{S}$ (diamonds), and $^{13}\text{C}^{34}\text{S}$ (downward triangles). For most of these IR transitions for $^{12}\text{C}^{33}\text{S}$ and $^{12}\text{C}^{34}\text{S}$, the differences are within 0.0002 cm^{-1} . From Figure 2(d), it is clear that there is an outlier ($\delta = 0.0003 \text{ cm}^{-1}$) for pure rotational transitions of $^{12}\text{C}^{34}\text{S}$ at a transition frequency of around 11 cm^{-1} , which corresponds to the R(6) transition of $\nu = 4-4$ of $^{12}\text{C}^{34}\text{S}$. Such obvious outliers are excluded in potential fitting.

2.2. Dipole Moment Function

Permanent dipole moment functions are investigated with the MRCI (Knowles & Werner 1988; Werner & Knowles 1988) and ACPF (Gdanitz & Ahlrichs 1988; Werner & Knowles 1990) approaches. The wave functions from state-averaged complete active space self-consistent field (CASSCF; Knowles & Werner 1985; Werner & Knowles 1985) calculations are used as reference wave functions for the MRCI and ACPF calculations. The active, doubly occupied, and frozen/core spaces are the same as those of the corresponding CASSCF calculations.

For the ground state of CS, the 22 electrons are distributed in 11 MOs, with an orbital energy order at equilibrium geometry of $[1\sigma^2 2\sigma^2 3\sigma^2 4\sigma^2 1\pi^4] 5\sigma^2 6\sigma^2 7\sigma^2 2\pi^4$. The

electronic configuration can be expressed as $(7a_1, 2b_1, 2b_2, 0a_2)$ (more compactly (7, 2, 2)) using the irreducible representations of the C_{2v} point group. Core orbitals (indicated in square brackets) are doubly occupied and frozen in all CASSCF, MRCI, and ACPF calculations in this work. All of the ab initio computations are performed with the MOLPRO package (Werner et al. 2015, 2012) and the basis sets (Dunning 1989; Kendall et al. 1992; Woon & Dunning 1993) embedded in it.

To obtain the optimized results from MRCI calculations, the dipole moments at R_e (1.5349 Å) are systematically investigated with different basis sets and active spaces of electronic configuration. Finally, we find that the electronic configuration space of $(12a_1, 4b_1, 4b_2, 1a_2)$ with the cc-pv5z (v5z) basis sets can produce the best dipole moment functions. In this configuration, the $2s2p3s$ shells of C and $3s3p3d4s$ shells of S atoms are put into the active space, which correspond to 15 MOs, i.e., $(8a_1, 3b_1, 3b_2, 1a_2)$ of the CS molecule. The rest of the electrons are put into the six closed-shell core orbitals. In total, 10 valence electrons are put into 15 active orbitals, 549,673 configuration state functions (CSFs) are generated in the CASSCF reference space, and 5,895,377 CSFs are involved in the MRCI calculations.

With the above electronic configuration, the obtained dipole moment at R_e (1.5349 Å) of the MRCI approach with v5z basis sets is 1.959 D, which is nearly identical to the experimental data 1.958(5) D (Winnewisser & Cook 1968). With the same configuration, the aug-cc-pvqz (avqz; 1.961 D) and aug-cc-pvqz-dk (avqz-dk; 1.964 D) basis sets also produce very good results at R_e , but the dipole moment functions in the long ranges seem not as good as those of the v5z data. The MRCI/v5z dipole moments are smooth in the range from 0.6 to about 3.0 Å. For $R > 3.4$ Å, the dipole functions are smooth, but the sign of the function is changed; see Figure 3. Similar to those of Ornellas (1998), which are plotted in Figure 3 for comparison, there are also two points of zero dipole moments apparent in $R < 3.4$ Å. The ACPF approach with avqz-dk basis sets produces similar results, except for those at around $R = 3.2$ and 3.9 Å, which look like outliers. Both the MRCI/v5z (circles) and ACPF/avqz-dk (plus signs) results are plotted in Figure 3. From Figure 3, it is clear that the data of $R \approx 3.1-3.4$ Å from MRCI calculations are slightly better than the ACPF results.

The dipole moment functions in the range of $R = 0.7-3.0$ Å have already covered most of the vibrational states up to ν_0 . However, since the function of $R > 3.0$ is still needed in numerical integrals, the dipole moment functions are refined by fitting the MRCI/v5z dipole moments using different polynomials separately. Note that besides the excellent dipole moment at R_e , the MRCI/v5z approach also produces a high-quality molecular potential, as shown in Figure 1. The ACPF/avqz-dk potential is also listed in Figure 1 for comparison, which is similar to the (MRCI+Q)/v5z results with the same electronic configuration.

For ease of obtaining reliable analytical functions, the dipole moments in the range of $R = 0.7-5$ Å are refined with three different expansions. In $R = 0.7-2.0$ Å, the dipole moments are fitted with a function in the form of a Padé approximant as

$$M(x) = M_0 \frac{(1+x)^3}{1 + \sum_{i=1}^7 a_i x^i}, \quad (10)$$

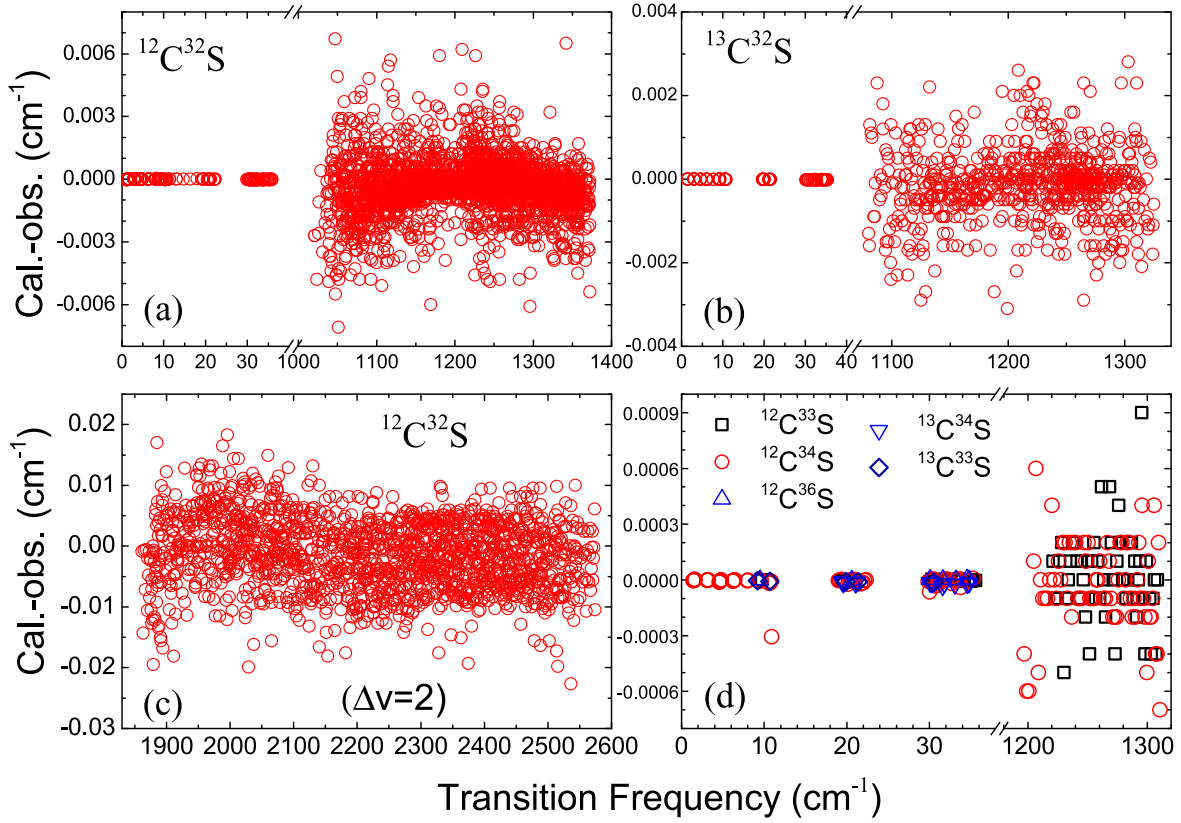


Figure 2. Comparison between observed and calculated transitions from the EMO potential for isotopologues of CS in the $X^1\Sigma^+$ state. Panels (a) and (b) are for the $\Delta v = 0$ and 1 bands of $^{12}\text{C}^{32}\text{S}$ and $^{13}\text{C}^{32}\text{S}$, respectively; (c) is for the overtone transitions of $\Delta v = 2$, $v = 0-28$ bands of $^{12}\text{C}^{32}\text{S}$; and (d) is for the pure rotational and rovibrational transitions of $^{12}\text{C}^{33}\text{S}$ (squares), $^{12}\text{C}^{34}\text{S}$ (circles), $^{12}\text{C}^{36}\text{S}$ (upward triangles), $^{13}\text{C}^{33}\text{S}$ (diamonds), and $^{13}\text{C}^{34}\text{S}$ (downward triangles).

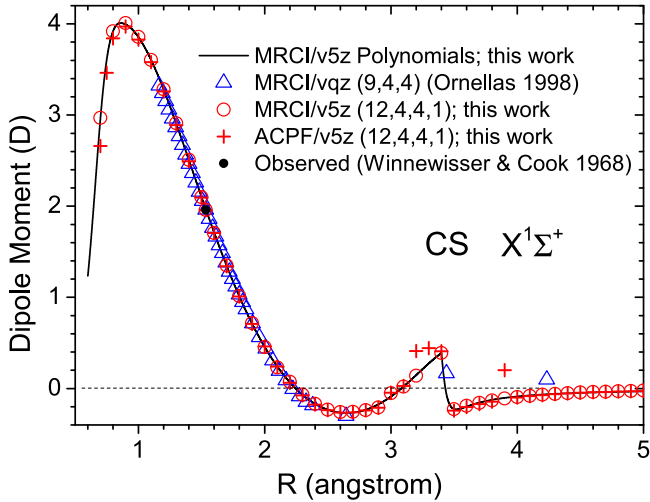


Figure 3. Dipole moment functions for CS from ab initio approaches. The refined dipole moment functions, i.e., MRCI/v5z polynomials (solid line), are used in the final line list calculation, which includes three different functions listed in Table 3. All ab initio data (MRCI, circles; ACPF, plus signs) are calculated with MOLPRO. The observed data (black points) are from Winniewisser & Cook (1968). Literature data (triangles) from Ornellas (1998) are also listed for comparison. The dashed line indicates that the dipole moments are zero on the curve.

in which $x = (R - R_e)/R_e$, M_0 is the dipole moment at R_e , and a_i are the fitting coefficients. The M_0 value was set to 1.958 D, which corresponds to the observed data at experimental R_e . The corresponding a_i coefficients, which are obtained with least-squares fitting, are listed in Table 3.

In $R = 1.0-3.4$ Å, the dipole moments are fitted with a polynomial,

$$M(R) = \sum_{i=0}^7 a_i R^i. \quad (11)$$

For $R = 3.4-5.0$ Å, another Padé function is used in fitting:

$$M(R) = \frac{a_0 + a_1 R^2}{1 + a_2 R^2 + a_3 R^4}. \quad (12)$$

The fitted parameters of Equations (10)–(12) for the MRCI/v5z dipole moments are listed in Table 3. Ab initio dipole moments and fitted functions are plotted in Figure 3. Results show that there is a cross at $R = 0.8487$ Å between the Padé function (Equation (10)) and the polynomial function (Equation (11)), whereas for Equations (11) and (12), the cross is at $R = 3.4$ Å. Therefore, for $R < 0.8487$ and > 3.4 Å, Equations (10) and (12) are used in the dipole moment polynomials, respectively. In the range from $R = 0.6$ to 3.4 Å, it can be found from Figure 3 that the refined dipole moment functions are smooth and can be used to represent the MRCI/v5z dipole moments very well. In the final line list calculations, such MRCI/v5z polynomials are used to predict the transition intensities for all eight isotopologues of the CS ground state.

For the MRCI dipole moments, although the main body of the MRCI/v5z polynomials in the range of $0.8487 \text{ Å} \leq R \leq 3.4 \text{ Å}$ already covers almost all of the bound levels, the dipole moment functions for $R < 0.8487$ and $> 3.4 \text{ Å}$ are still needed (integrated from 0.6 to 18.6 Å in LEVEL, with step

Table 3
Refined Dipole Moment Functions for the $X^1\Sigma^+$ State of CS^a

Functions	Equation (10)	Equation (11) ^b	Equation (12) ^b
Application	$R < 0.8487 \text{ \AA}$	$R = 0.8487\text{--}3.4 \text{ \AA}$	$R > 3.4 \text{ \AA}$
M_0	1.958 D (Fixed)
a_0	...	-5.60521781618336	0.0398739421269425
a_1	6.09392887406335	25.2210371786645	-0.00338665800914841
a_2	22.0511373816226	-16.0415455294694	-0.175118847480934
a_3	69.6642512188976	-6.87877899079566	0.00767942504535742
a_4	185.823239328245	11.0826360489514	...
a_5	330.749501200133	-4.77955418448756	...
a_6	316.093622725595	0.927620790359716	...
a_7	116.429946474375	-0.0697494802400968	...

Notes.

^a Polynomials are fitted with dipole moments at the MRCI/v5z ($12a_1$, $4b_1$, $4b_2$, $1a_2$) level.

^b Dipole moment in units D and R in units \AA .

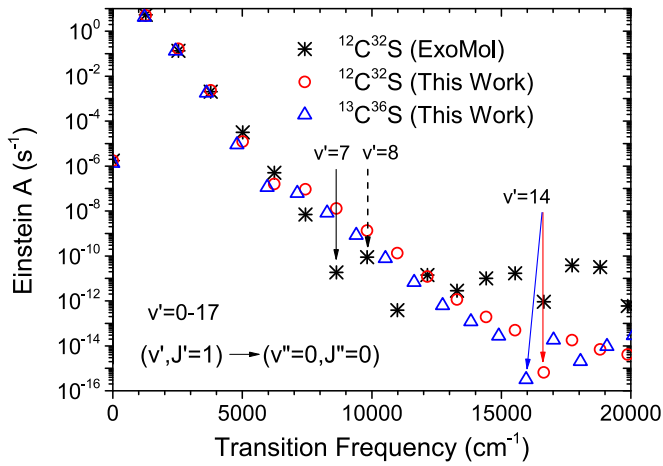


Figure 4. Einstein A coefficients for overtone transitions to the lowest vibration-rotation state ($v'' = 0$, $J'' = 0$) for $^{12}\text{C}^{32}\text{S}$ (circles) and $^{13}\text{C}^{36}\text{S}$ (triangles) from EMO potential and refined dipole moment functions (MRCI/v5z polynomials). The reproduced ExoMol data (Paulose et al. 2015; asterisks) are also listed for comparison. Solid arrows indicate the highest-overtone transitions and corresponding frequencies with normal intensity distributions for each isotopologue. The dashed arrow shows that the Einstein A of the transition of $\Delta v = 8$ is already greater than that of $\Delta v = 7$.

size 0.0002 \AA) and are therefore used in the following calculations.

The Einstein A values from the refined dipole moment functions are displayed in Figure 4 for transitions of ($v' = 1\text{--}17$, $J = 1$)–($v'' = 0$, $J'' = 0$) for $^{12}\text{C}^{32}\text{S}$ (circles) and $^{13}\text{C}^{36}\text{S}$ (triangles). Figure 4 indicates that the MRCI/v5z polynomials (results of the present work) can be used to produce high-overtone transitions up to about $16,600 \text{ cm}^{-1}$ for $^{12}\text{C}^{32}\text{S}$, which corresponds to $v' = 14$ (also $\Delta v = 14$) and is indicated with a vertical arrow in the figure. In the range over this frequency, the intensities abnormally increase with higher transition frequencies. This demonstrates that the refined dipole moment functions (MRCI/v5z polynomials) can be used to produce physically reasonable intensity distributions for high-overtone transitions in the CS ground electronic state.

For $^{12}\text{C}^{32}\text{S}$, the results of Paulose et al. (2015; ExoMol; asterisks), which are recalculated with the downloaded input file of LEVEL, are also listed in Figure 4 for comparison. For $\Delta v = 0\text{--}1$, the present results agree well with the ExoMol data.

For higher-overtone transitions, the discrepancies increase to a maximum at $v' = 7$ (solid arrow). For $v' > 7$, abnormal data (e.g., ($v' = 8$, $J = 1$)–($v'' = 0$, $J'' = 0$); dashed arrow) begin to appear. Such a comparison indicates that the intensity from the Einstein A values of the ExoMol data should fundamentally agree with the present results for transitions, at least in the range of $\Delta v = 0\text{--}3$. Details on the ExoMol intensities will be discussed later.

For the heaviest isotopologue studied in this work, $^{13}\text{C}^{36}\text{S}$, the normal intensities from MRCI/v5z polynomials are up to a frequency close to $16,000 \text{ cm}^{-1}$, which also corresponds to $\Delta v = 14$ ($v' = 14$) in Figure 4 and is indicated with a solid arrow. To obtain safety predictions of transition intensities for all isotopologues, only transitions within $15,000 \text{ cm}^{-1}$ are kept. Such frequencies also span nearly all transitions of $0 \leq \Delta v \leq 12$, $\Delta J = \pm 1$ in $v = 0\text{--}59$, $J_{\text{max}} = 157\text{--}260$ for isotopologues from $^{12}\text{C}^{32}\text{S}$ to $^{13}\text{C}^{36}\text{S}$.

2.3. Line Lists

Rotation-vibration line lists are obtained with the effective EMO potential listed in Table 2 by direct solution of the Schrödinger Equation (1) for nuclear motion using the LEVEL (LeRoy 2017b) program. LEVEL also produces transitional dipole moment matrix elements (TDMs), the corresponding Einstein A values for each line, and a set of band constants (B_v , D_v , H_v , ..., O_v) for each vibrational level. These band constants are useful for simulating spectra with a program such as PGOPHER (Western 2017).

In the range of the observed transitions, most of the differences in the observed frequencies are within $0.0005\text{--}0.005 \text{ cm}^{-1}$ for the computed transitions of $\Delta v = 1$, which are close to most of the estimated experimental uncertainties. The rms errors for $^{12}\text{C}^{32}\text{S}$ (4595), $^{13}\text{C}^{32}\text{S}$ (772), $^{12}\text{C}^{33}\text{S}$ (70), and $^{12}\text{C}^{34}\text{S}$ (158) are 0.0037, 0.0008, 0.0002, and 0.0002 cm^{-1} , respectively. Data in parentheses are the total numbers of observed data available for comparison, which are slightly larger than the data used in the fit. For the $\Delta v = 2$ overtone transitions of $^{12}\text{C}^{32}\text{S}$ (1770), the rms is 0.0057 cm^{-1} ; for most of the computed transition frequencies, the differences in the observed data are within 0.01 cm^{-1} . For transitions of $\Delta v = 0$ and 1 of $^{12}\text{C}^{32}\text{S}$ (2825), the corresponding rms is 0.0014 cm^{-1} .

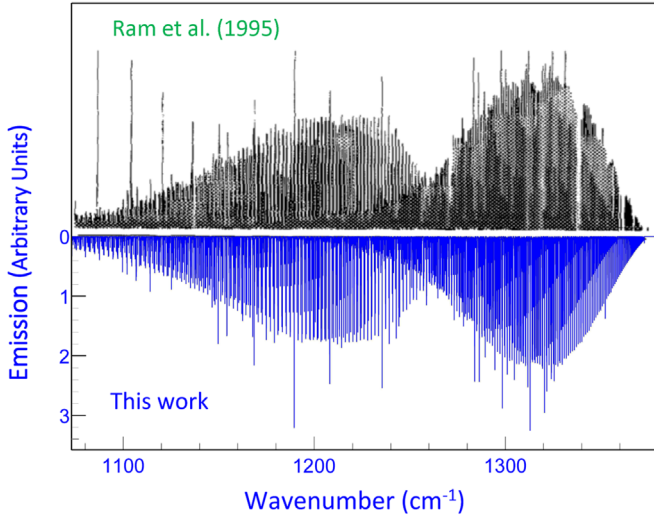


Figure 5. Overall comparison between observed and calculated spectra of $^{12}\text{C}^{32}\text{S}$ at 2573 K. Observed data (upper) are taken from Ram et al. (1995), and calculated data (lower; the present work) are obtained with PGOPHER using results from MRCI/v5z potential functions. See Tables 2 and 3 for details on the molecular potential and dipole moment.

The intensity of a line as measured by the Einstein A value is given by the expression (Bernath 2016; LeRoy 2017b)

$$A_{J' \rightarrow J''} = 3.1361889 \times 10^{-7} \frac{S(J', J'')}{2J' + 1} \tilde{\nu}^3 \langle \Psi_{v'J'} | M(r) | \Psi_{v''J''} \rangle^2, \quad (13)$$

in which A is in s^{-1} units, $M(r)$ is the dipole moment function in D, $\tilde{\nu}$ is the transition frequency in cm^{-1} , $S(J', J'')$ is a Hönl–London rotational factor, and $\Psi_{v'J'}$ and $\Psi_{v''J''}$ are the vibration-rotational wave functions that depend on the effective molecular potential function (Bernath 2016). Based on the calculated Einstein A factors (in s^{-1}) and transition frequency $\tilde{\nu}$ (in cm^{-1}), the oscillator strengths $f_{J' \leftarrow J''}$ have been calculated with the following relationship (Bernath 2016):

$$f_{J' \leftarrow J''} = 1.4991938 \frac{1}{2\tilde{\nu}^2} \frac{(2J' + 1)}{(2J'' + 1)} A_{J' \rightarrow J''}. \quad (14)$$

From Equation (13), the two factors that influence the vibration-rotation line intensities in an electronic state are the wave functions Ψ_{vJ} , determined by the effective potential, and the dipole moment function $M(r)$. In this work, the dipole moments are assumed to be isotope-invariant. The refined dipole moment functions (listed in Table 3), i.e., the MRCI/v5z polynomials in the forms of Equations (10)–(12), are used in TDM calculations.

These intensities (in units of $\text{s}^{-1} \text{ molecule}^{-1}$) can be estimated as relative photon emission rates (Bernath 2016),

$$I = A \left(\frac{g_{\text{upper}}}{Q} e^{-\frac{E_{\text{upper}}}{kT}} \right), \quad (15)$$

in which Q is the partition function, A is the Einstein A coefficient (s^{-1}), and g_{upper} is the upper-state degeneracy. The calculated emission line intensities, I , which are simulated for $^{12}\text{C}^{32}\text{S}$ (at 2573 K) using the calculated Einstein A with the PGOPHER program, are presented in Figure 5 (in the range of 1080–1370 cm^{-1}) as an overview and Figure 6 for a short

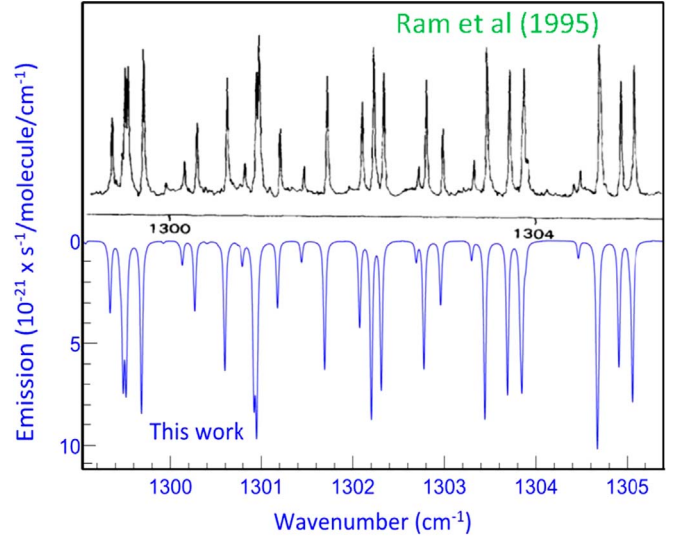


Figure 6. Comparison between observed and simulated intensities for a small portion of emissions of $^{12}\text{C}^{32}\text{S}$ at 2573 K. The observed spectrum (upper) is taken from Ram et al. (1995). Simulated data (lower; the present work) are the same as those in Figure 5.

segment of the observed spectrum (Ram et al. 1995). The positions and relative intensities agree excellently with the observed data, as shown in Figures 5 and 6. This demonstrates that the dipole moment and analytical EMO potential can be used to represent the observed spectrum very well.

For convenience of comparing with results in other databases, such as the CDMS (Müller et al. 2005) data, these absorption intensities (in units of $\text{nm}^2 \text{ MHz}$) are calculated using the following relationship (Pickett et al. 1998):

$$I(\text{nm}^2 \text{ MHz}) = 3.75602 \times 10^{15} A \frac{1}{\nu^2} \frac{g_{\text{upper}}}{Q} \left(e^{-\frac{E_{\text{lower}}}{kT}} - e^{-\frac{E_{\text{upper}}}{kT}} \right), \quad (16)$$

in which A is in s^{-1} , and ν is the frequency in MHz.

For $^{12}\text{C}^{32}\text{S}$, the simulated intensities from databases such as CDMS and ExoMol are also directly compared with the present data. The detailed results at a temperature of 300 K for bands of $\nu = 0-0$, $1-0$, $2-1$, and $2-0$ are presented in Figure 7. For the $\nu = 0-0$ band (see Figure 7(a)), the present data (circles) agree excellently with the CDMS (squares) and ExoMol (triangles) data. For bands of $\nu = 1-0$ (Figure 7(b)) and $2-1$ (Figure 7(c)), the present results also agree well with the CDMS and ExoMol data, and the differences are within about 10% for those strongest transitions. For the $\nu = 2-0$ band, as shown in Figure 7(d), such differences are increased to about 20%. This means that the TDMs of the ExoMol and CDMS data are also in an agreement of about 90% with the present work. For higher-overtone transitions, it can be expected from the Einstein A values shown in Figure 4 that the differences between the intensities of the present data and those of the ExoMol data will increase according to the increasing $\Delta\nu$ (up to $\Delta\nu = 7$).

Final line lists of eight isotopologues of CS, including $^{12}\text{C}^{32}\text{S}$, $^{12}\text{C}^{33}\text{S}$, $^{12}\text{C}^{34}\text{S}$, $^{12}\text{C}^{36}\text{S}$, $^{13}\text{C}^{32}\text{S}$, $^{13}\text{C}^{33}\text{S}$, $^{13}\text{C}^{34}\text{S}$, and $^{13}\text{C}^{36}\text{S}$, for transitions within 15,000 cm^{-1} are predicted. Such line lists also cover most of the transitions satisfying the dipole selection rule $\Delta J = \pm 1$, within $\Delta\nu \leq 12$, in the range of $\nu = 0-59$ and J up to $J_{\text{max}} = 157-260$. The band constants for

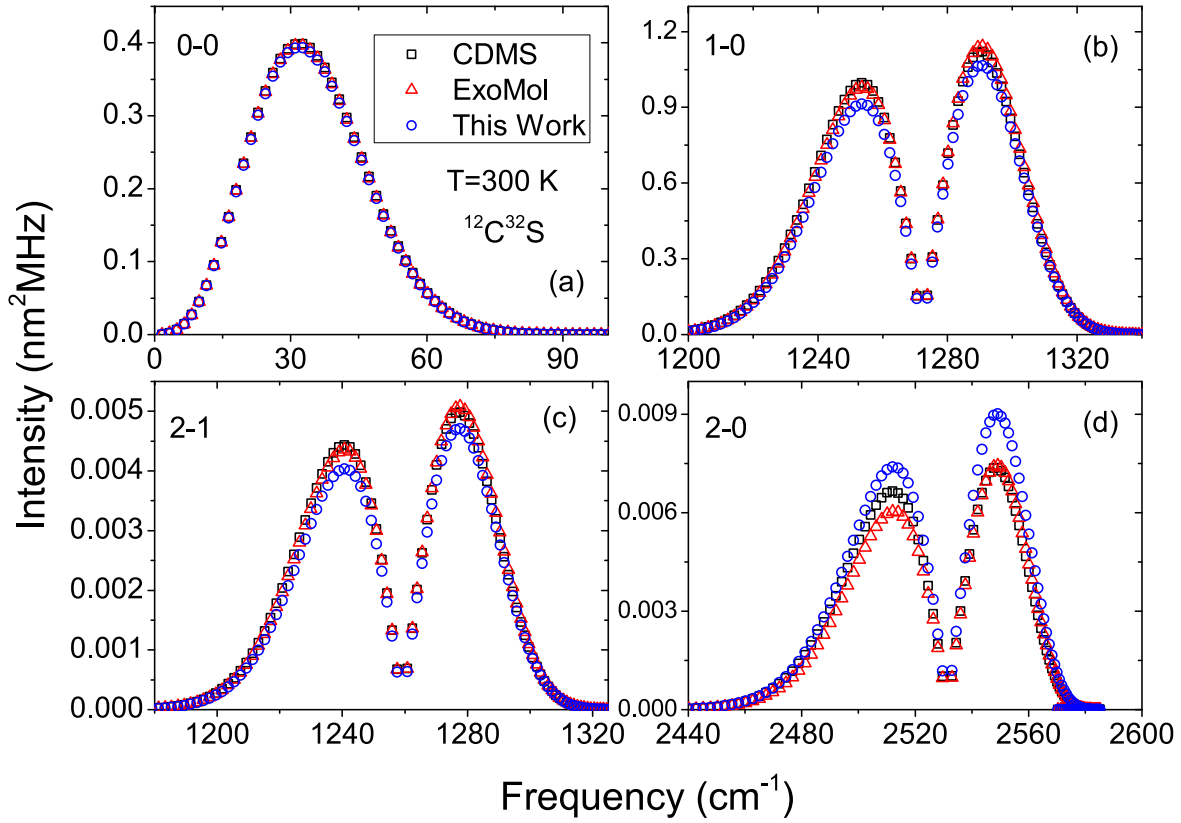


Figure 7. Comparison between simulated transition intensities of the $\nu = 0-0$, $1-0$, $2-1$, and $2-0$ bands for $^{12}\text{C}^{32}\text{S}$ at 300 K. Squares indicate the CDMS results from Müller et al. (2005); triangles indicate the ExoMol data (Paulose et al. 2015), which are recalculated with their input file for LEVEL; and circles indicate data from the present work.

Table 4
Band Constants (in cm^{-1}) for the $X^1\Sigma^+$ State of CS Isotopologues

Species	ν	Gv	Bv	$-Dv \times 10^6$	$Hv \times 10^{13}$	$Lv \times 10^{18}$	$Mv \times 10^{24}$	$Nv \times 10^{29}$	Ov
$^{12}\text{C}^{32}\text{S}$	0	0	0.81708407	-1.3363846	2.4052851	-2.3172608	-4.9584573	-2.5206067	$-1.1027019 \times 10^{-34}$
$^{12}\text{C}^{32}\text{S}$	1	1272.1621	0.811163635	-1.3377917	2.2343626	-2.3889654	-5.3397284	-2.7836835	$-1.0402058 \times 10^{-34}$
$^{12}\text{C}^{33}\text{S}$	0	0	0.810338429	-1.3143684	2.3464004	-2.2414003	-4.7560482	-2.3975772	$-9.8433697 \times 10^{-35}$
$^{12}\text{C}^{33}\text{S}$	1	1266.9436	0.804491292	-1.3157463	2.1803958	-2.3104531	-5.1202019	-2.6467624	$-8.8827640 \times 10^{-35}$
$^{12}\text{C}^{34}\text{S}$	0	0	0.804007909	-1.2938738	2.2920188	-2.1719201	-4.5721725	-2.2867177	$-7.3500348 \times 10^{-35}$
$^{12}\text{C}^{34}\text{S}$	1	1262.0262	0.798229279	-1.2952246	2.1305364	-2.2385546	-4.9208416	-2.5234331	$-6.9093787 \times 10^{-35}$
$^{12}\text{C}^{36}\text{S}$	0	0	0.792363729	-1.2565983	2.1941922	-2.0483605	-4.2488538	-2.0939688	$-6.5166107 \times 10^{-35}$
$^{12}\text{C}^{36}\text{S}$	1	1252.9294	0.786710403	-1.2579002	2.0407960	-2.1107199	-4.5704506	-2.3091275	$-5.8440579 \times 10^{-35}$
$^{13}\text{C}^{32}\text{S}$	0	0	0.771328407	-1.1906460	2.0261304	-1.8388614	-3.7109140	-1.7801074	$-1.2232180 \times 10^{-34}$
$^{13}\text{C}^{32}\text{S}$	1	1236.3159	0.765899206	-1.1918619	1.8865887	-1.8940445	-3.9879780	-1.9605276	$-1.1533845 \times 10^{-34}$
$^{13}\text{C}^{33}\text{S}$	0	0	0.764581609	-1.1698698	1.9735977	-1.7751346	-3.5506003	-1.6881799	$-1.0909627 \times 10^{-34}$
$^{13}\text{C}^{33}\text{S}$	1	1230.9409	0.759223611	-1.1710590	1.8383063	-1.8281579	-3.8145034	-1.8585213	$-9.8372243 \times 10^{-35}$
$^{13}\text{C}^{34}\text{S}$	0	0	0.758249998	-1.1505390	1.9251290	-1.7168526	-3.4052482	-1.6055476	$-8.1280410 \times 10^{-35}$
$^{13}\text{C}^{34}\text{S}$	1	1225.8743	0.752958535	-1.1517034	1.7937414	-1.7679097	-3.6572718	-1.7668623	$-7.6372460 \times 10^{-35}$
$^{13}\text{C}^{36}\text{S}$	0	0	0.746603803	-1.1154040	1.8380568	-1.6134178	-3.1503606	-1.4623630	$-7.1996651 \times 10^{-35}$
$^{13}\text{C}^{36}\text{S}$	1	1216.4993	0.741433991	-1.1165237	1.7136377	-1.6610074	-3.3816763	-1.6081456	$-6.4517792 \times 10^{-35}$

(This table is available in its entirety in machine-readable form.)

$\nu = 0-59$ and $J = 0$ are collected in Table 4. The transition file, including transition frequencies $\tilde{\nu}$, Einstein A factors, oscillator strength f , and TDMs, etc. for $^{12}\text{C}^{32}\text{S}$, $^{12}\text{C}^{33}\text{S}$, $^{12}\text{C}^{34}\text{S}$, $^{12}\text{C}^{36}\text{S}$, $^{13}\text{C}^{32}\text{S}$, $^{13}\text{C}^{33}\text{S}$, $^{13}\text{C}^{34}\text{S}$, and $^{13}\text{C}^{36}\text{S}$ are presented in Table 5. The state file, including energy levels of each isotopologue, which are sorted and assigned with a unique state counting number (state ID), are presented in Table 6 in ExoMol format. Details about the formats of the ExoMol line list files

can be obtained in Tennyson et al. (2016). Line lists for each isotopologue contain around 448,000–475,000 transitions. Over 3,692,000 lines with transition intensities are predicted in total.

2.4. Partition Function

The partition functions have been tested with rovibrational levels up to the dissociation limit, including quasibound levels

Table 5
Einstein A Coefficients, Oscillator Strengths, and TDMs for Transitions of the $X^1\Sigma^+$ State of CS Isotopologues

Species	ID_U ^a	ID_L ^a	$A_{J' \rightarrow J''}(\text{s}^{-1})$	$f_{J' \leftarrow J''}$	TDMs (D)	$\tilde{\nu}$ (cm ⁻¹)	Assignment
¹² C ³² S	8875	8874	1.722×10^{-7}	5.163×10^{-7}	9.469×10^{-1}	1.22473	R(0) $\nu = 34-34$
¹² C ³² S	1398	1138	1.691×10^1	2.381×10^{-5}	-3.150×10^{-1}	1026.28528	P(93) $\nu = 5-4$
¹² C ³² S	2422	2160	6.615×10^1	6.471×10^{-5}	-4.683×10^{-1}	1246.54736	R(71) $\nu = 9-8$
¹² C ³² S	374	112	1.139×10^1	9.148×10^{-6}	-1.680×10^{-1}	1372.50903	R(111) $\nu = 1-0$
¹² C ³² S	7333	6810	5.210×10^1	2.271×10^{-5}	2.235×10^{-1}	1893.74792	R(23) $\nu = 28-26$
¹² C ³² S	4213	3692	1.785×10^1	5.892×10^{-6}	1.099×10^{-1}	2102.45459	P(37) $\nu = 16-14$
...
¹² C ³³ S	545	544	2.345×10^{-2}	2.990×10^{-5}	1.882×10^0	35.08416	R(21) $\nu = 2-2$
¹² C ³³ S	284	283	2.476×10^{-2}	3.111×10^{-5}	1.913×10^0	35.34158	R(21) $\nu = 1-1$
¹² C ³³ S	287	27	6.474×10^0	6.264×10^{-6}	-1.491×10^{-1}	1221.09729	P(26) $\nu = 1-0$
¹² C ³⁴ S	4178	4177	6.461×10^{-7}	1.436×10^{-6}	1.465×10^0	1.42237	R(0) $\nu = 16-16$
¹² C ³⁴ S	2096	2095	5.072×10^{-4}	7.800×10^{-6}	1.704×10^0	10.60618	R(6) $\nu = 8-8$
¹² C ³⁴ S	297	37	5.954×10^0	6.058×10^{-6}	-1.477×10^{-1}	1197.09583	P(36) $\nu = 1-0$
¹² C ³⁶ S	284	283	2.317×10^{-2}	3.044×10^{-5}	1.913×10^0	34.56169	R(21) $\nu = 1-1$
¹² C ³⁶ S	23	22	2.444×10^{-2}	3.164×10^{-5}	1.944×10^0	34.81049	R(21) $\nu = 0-0$
¹³ C ³² S	1327	1326	1.500×10^{-2}	2.422×10^{-5}	1.795×10^0	31.21046	R(20) $\nu = 5-5$
¹³ C ³² S	341	81	4.019×10^0	5.092×10^{-6}	-1.420×10^{-1}	1080.97351	P(80) $\nu = 1-0$
¹³ C ³² S	609	347	1.823×10^1	1.606×10^{-5}	-2.275×10^{-1}	1312.06604	R(85) $\nu = 2-1$
¹³ C ³³ S	15	14	5.621×10^{-3}	1.977×10^{-5}	1.947×10^0	21.39544	R(13) $\nu = 0-0$
¹³ C ³³ S	21	20	1.650×10^{-2}	2.786×10^{-5}	1.945×10^0	30.54583	R(19) $\nu = 0-0$
¹³ C ³⁴ S	536	535	3.947×10^{-3}	1.693×10^{-5}	1.888×10^0	19.42916	R(12) $\nu = 2-2$
¹³ C ³⁴ S	24	23	2.449×10^{-2}	3.163×10^{-5}	1.944×10^0	34.82351	R(22) $\nu = 0-0$
...
¹³ C ³⁶ S	284	283	1.944×10^{-2}	2.874×10^{-5}	1.915×10^0	32.57555	R(21) $\nu = 1-1$
¹³ C ³⁶ S	23	22	2.046×10^{-2}	2.984×10^{-5}	1.945×10^0	32.80307	R(21) $\nu = 0-0$

Note.

^a ID_U and ID_L indicate the upper- and lower-state ID, respectively.

(This table is available in its entirety in machine-readable form.)

Table 6

Energy Levels and State Counting Number (State ID) for the $X^1\Sigma^+$ State of CS Isotopologues in ExoMol Format

Species	State ID	$E_{v,J}$ (cm ⁻¹)	g^a	J	ν
¹² C ³² S	1	0	1	0	0
¹² C ³² S	2	1.634163	3	1	0
¹² C ³² S	3	4.902456	5	2	0
...
¹² C ³² S	14329	62093.51455	315	157	59
¹² C ³² S	14330	62164.95311	317	158	59
¹² C ³³ S	1	0	1	0	0
¹² C ³³ S	2	1.620671	3	1	0
...
¹² C ³³ S	14375	62086.29104	317	158	59
¹² C ³³ S	14376	62160.75744	319	159	59
...
¹³ C ³⁶ S	14774	62613.17417	353	176	59
¹³ C ³⁶ S	14775	62691.72215	355	177	59

Note.

^a $g = (2J+1)$ is the state degeneracy.

(This table is available in its entirety in machine-readable form.)

by

$$Q = \sum_{\nu=0}^{\nu_{\max}} \left[\sum_{J=0}^{J_{\max}} (2J+1) e^{\left(-\frac{E_{\nu,J}}{k_B T}\right)} \right], \quad (17)$$

where $E_{\nu,J}$ is relative to the ZPE. For ¹²C³²S, the maximum vibrational level is $\nu_{\max} = 81$, for which $J_{\max} = 0$; the maximum rotational level is $J_{\max} = 369$, which corresponds to the vibrational

level $\nu = 0$. For $T = 150, 300, 500, 1000, 2000$, and 3000 K, the partition functions $Q(T)$ are close to those (in parentheses) of Paulose et al. (2015), which are 127.9821 (127.9828), 256.3141 (256.3165), 437.5877 (437.5903), 1018.47 (1018.57), 2881.07 (2880.03), and 5741.48 (5705.8), respectively. Because of such a high similarity, it can be expected that the fitted analytical partition functions by Paulose et al. (2015) can be adopted with a rather high accuracy for most of the temperatures under 3000 K. In this work, the partition functions are calculated in the temperature range of $T = 10-7500$ K in steps of 10 K. A series expansion that is the same as that of Paulose et al. (2015) for partition functions is therefore fitted again for ease of use:

$$\log_{10} Q(T) = \sum_{n=0}^7 b_n (\log_{10} T)^n. \quad (18)$$

The calculated partition functions and the determined b_n coefficients are provided in Tables 7 and 8, respectively.

3. Discussion

The empirical EMO potential function for the CS ground state is obtained by fitting with the latest observed frequencies of ¹²C³²S, ¹²C³³S, ¹²C³⁴S, and ¹³C³²S. In the range of $\nu = 0-28$, the predicted transitions are in high agreement with the observed data. The comparison with the MRCI/v5z potential indicates that the EMO potential also agrees well with the high-level ab initio data in the long range. For comparison, a potential was also fitted with part of the transitions listed in Table 1, in which the data of Kawaguchi & Deo (2019) were excluded. From that potential (parameter set

Table 7
Partition Functions $Q(T)$ for the $X^1\Sigma^+$ State of CS Isotopologues

T (K)	$^{12}\text{C}^{32}\text{S}$	$^{12}\text{C}^{33}\text{S}$	$^{12}\text{C}^{34}\text{S}$	$^{12}\text{C}^{36}\text{S}$	$^{13}\text{C}^{32}\text{S}$	$^{13}\text{C}^{33}\text{S}$	$^{13}\text{C}^{34}\text{S}$	$^{13}\text{C}^{36}\text{S}$
100	8.5421×10^1	8.6129×10^1	8.6804×10^1	8.8075×10^1	9.0468×10^1	9.1263×10^1	9.2023×10^1	9.3453×10^1
500	4.3759×10^2	4.4140×10^2	4.4505×10^2	4.5191×10^2	4.6487×10^2	4.6918×10^2	4.7331×10^2	4.8108×10^2
1000	1.0185×10^3	1.0284×10^3	1.0380×10^3	1.0559×10^3	1.0900×10^3	1.1013×10^3	1.1122×10^3	1.1328×10^3
2000	2.8811×10^3	2.9124×10^3	2.9425×10^3	2.9992×10^3	3.1068×10^3	3.1427×10^3	3.1772×10^3	3.2424×10^3
3000	5.7415×10^3	5.8068×10^3	5.8693×10^3	5.9874×10^3	6.2117×10^3	6.2868×10^3	6.3587×10^3	6.4949×10^3
4000	9.6460×10^3	9.7583×10^3	9.8658×10^3	1.0069×10^4	1.0455×10^4	1.0584×10^4	1.0708×10^4	1.0943×10^4
5000	1.4643×10^4	1.4816×10^4	1.4981×10^4	1.5294×10^4	1.5889×10^4	1.6088×10^4	1.6279×10^4	1.6641×10^4
6000	2.0787×10^4	2.1035×10^4	2.1272×10^4	2.1721×10^4	2.2573×10^4	2.2859×10^4	2.3133×10^4	2.3652×10^4
7000	2.8141×10^4	2.8479×10^4	2.8802×10^4	2.9414×10^4	3.0577×10^4	3.0966×10^4	3.1340×10^4	3.2047×10^4
7500	3.2294×10^4	3.2683×10^4	3.3055×10^4	3.3759×10^4	3.5097×10^4	3.5545×10^4	3.5975×10^4	3.6789×10^4

(This table is available in its entirety in machine-readable form.)

Table 8
Fitted Parameters for Analytic Partition Functions of the CS $X^1\Sigma^+$ State in 10–7500 K

	$^{12}\text{C}^{32}\text{S}$	$^{12}\text{C}^{33}\text{S}$	$^{12}\text{C}^{34}\text{S}$	$^{12}\text{C}^{36}\text{S}$	$^{13}\text{C}^{32}\text{S}$	$^{13}\text{C}^{33}\text{S}$	$^{13}\text{C}^{34}\text{S}$	$^{13}\text{C}^{36}\text{S}$
b_0	-7.949753	-7.927335	-7.90555	-7.867989	-7.785646	-7.756204	-7.728454	-7.677137
b_1	28.85408	28.79917	28.74444	28.65293	28.4402	28.36231	28.28815	28.15213
b_2	-40.17943	-40.11948	-40.05776	-39.95755	-39.71217	-39.62061	-39.53218	-39.37162
b_3	30.76017	30.7301	30.69718	30.64699	30.50988	30.45679	30.40445	30.31089
b_4	-13.52067	-13.51463	-13.50671	-13.49682	-13.45963	-13.44398	-13.42798	-13.40019
b_5	3.416005	3.416294	3.415959	3.416567	3.413013	3.410993	3.408724	3.405074
b_6	-0.4600901	-0.4603679	-0.4605426	-0.4610363	-0.4613255	-0.4613062	-0.461233	-0.4611836
b_7	0.02559541	0.02562372	0.02564525	0.02569496	0.02575222	0.02576464	0.02577299	0.02579391

$N = 7$, $p = m = 3$, $q_{\text{NA}} = 3$), the predicted transitions for $v = 0-9$ of $\Delta v = 0$, 1 are of the same quality as the present data; for transitions of $\Delta v = 2$, $v'' \leq 16$, the deviations of the predictions are similar to but slightly larger than the present results. For $v'' > 16$, the quality of the predictions is obviously less than the results of the present work, and the deviations to the observed transitions are increasing with extended vibrational levels; but the largest deviation of the predicted transition frequencies to the observed data of $v = 28-26$ is still not larger than 0.13 cm^{-1} . The results demonstrate that the predictions are accurate enough within the range of the observed vibrational and rotational levels; for transitions over the states of observed data, reliable predictions are still expected to a rather high extent. But the accuracy may decrease according to the increasing extended vibrational and rotational states.

Dipole moments are obtained with the MRCI approach, which gives the same dipole moment functions as the MRCI +Q method, since the Davidson correction (+Q) only modifies the calculated total energies. When the Davidson correction is considered in the total energy, the potential curve in the long range is similar to the present results of ACPF/avqz-dk (in Figure 1) with the same active space.

The basis sets (v5z) used in the present work are not as large as those of Pattillo et al. (2018; av6z), Shi et al. (2011; av5z and av6z), and Li et al. (2013b; aug-ccpwCV5Z); however, the configuration space (12, 4, 4, 1) is far larger than theirs (8, 3, 3). In addition, the combination of the present configuration space and basis sets can produce the best prediction for the dipole moment at R_e . Besides, the dipole moment functions are also the best in the long range. In fact, configuration spaces of (8, 3, 3), (9, 4, 4), (10, 4, 4), (10, 4, 4, 1), (11, 4, 4, 1), and (12,

4, 4, 1) with vqz, avqz, and v5z basis sets have also been tested systematically. For some of the relatively smaller configurations, the av5z and avqz-dk basis sets are also tried. The qualities of the dipole moments ($=1.926-2.005 \text{ D}$) at equilibrium are similar; the deviations from the experimental data are within $\pm 3\%$. However, the qualities of dipole moment functions in the long range are different. Among them, the MRCI/v5z with an electronic configuration of (12, 4, 4, 1) can produce the most smooth data up to around 3.4 \AA . Therefore, dipole moments at the MRCI/v5z (12, 4, 4, 1) level are used in the final line list calculations for isotopologues of CS.

For high-overtone transitions, it is known that numerical dipole moment functions may cause unphysical behaviors in the calculated intensities. For the CS ground state, the dipole moments (Figure 3) are not like some other molecules, such as HF, HCl, HI, MgF, etc., for which the dipole moments can be well expressed with an analytical function such as Padé approximant polynomials of Equation (10) (Li et al. 2013c; Hou & Bernath 2017). It is hard to fit the dipole moment curve in the range of $R > 2.2 \text{ \AA}$ with a simple analytical formula. To obtain analytical dipole moment functions for high-overtone transitions, polynomial functions in different forms (Table 3) are fitted with the MRCI/v5z dipole moments to avoid unexpected abnormal intensity distributions.

The plot of Einstein A values for $^{12}\text{C}^{32}\text{S}$ given in Figure 4 indicates that there are no obvious abnormal transition intensities up to about $16,600 \text{ cm}^{-1}$, which corresponds to overtone transitions of $\Delta v = 14$ or higher. Note that in Figure 4, only the transitions to state ($v'' = 0$, $J'' = 0$) are presented. Tests are also made for increasing v'' . Results indicate that the largest overtone transitions with normal intensities are increasing according to the increasing v'' . In the final line list calculations, only transitions less

than $15,000\text{ cm}^{-1}$ are produced, which covers most of the overtone transitions of $\Delta v \leq 12$. Such a span of overtone transitions is larger than the line lists of CS from the known literature, such as Pineiro et al. (1987; $\Delta v = 4$), Müller et al. (2005; CDMS; $\Delta v = 2$), and Paulose et al. (2015; ExoMol; $\Delta v = 9$). Therefore, the present line lists can enlarge the use of CS spectroscopic data in environments with various temperatures, especially in high-temperature astrophysical objects, in which molecules can be excited to very high rovibrational states.

Finally, we note that the predicted intensities of ExoMol results (Paulose et al. 2015) are also acceptable for lower-overtone transitions, as shown in Figures 4 and 7. This means that the obtained TMDs and Einstein A values of the ExoMol data have no problem. However, based on the quality of the data presented in Figures 4 and 7, it is hard to understand the results shown in Figure 5 of Paulose et al. (2015), in which the strongest lines (which correspond to the R(27)–R(31) of the $v = 2-1$ band) are about twice as strong as they should be when comparing with the experimental results. To deal with this problem, many tests have been made with the accessed input file of LEVEL of Paulose et al. (2015). At last, we found the produced transitions for $v'-(v''=1)$ and $v'-(v''=5)$ appearing twice; in addition, the transitions of $v'-(v''=15)$ were not available. Then it was noticed that in the last line of the input file to LEVEL, the vibrational quantum number 15 was separated into 1 and 5. This might cause the intensities to be overly high if the same lines were counted twice. For convenience of checking the calculated intensities of the present work, the assignment of each line is provided, along with the transition frequencies in Table 5.

4. Conclusions

The line lists for eight isotopologues of CS in the ground electronic state have been calculated using refined ab initio dipole moment functions. The calculated permanent dipole moment at R_e is identical to experimental data within the observation uncertainty. The predicted transition intensities with the refined analytical dipole moment functions are in excellent agreement with the observed spectrum at 2573 K. An empirical EMO potential including BOB modifications has been determined by DPF using over 4300 rovibrational and rotational transitions of $^{12}\text{C}^{32}\text{S}$, $^{12}\text{C}^{33}\text{S}$, $^{12}\text{C}^{34}\text{S}$, and $^{13}\text{C}^{32}\text{S}$. For most of the observed transitions of CS isotopologues, the differences between the calculated and observed frequencies agree within the observation uncertainties. All transitions within $15,000\text{ cm}^{-1}$ in the range of $v = 0-59$, $J_{\text{max}} \leq 260$, $\Delta v \leq 12$, and $\Delta J = \pm 1$ are predicted for $^{12}\text{C}^{32}\text{S}$, $^{12}\text{C}^{33}\text{S}$, $^{12}\text{C}^{34}\text{S}$, $^{13}\text{C}^{32}\text{S}$, $^{13}\text{C}^{33}\text{S}$, $^{13}\text{C}^{34}\text{S}$, and $^{13}\text{C}^{36}\text{S}$. Over 3,692,000 lines are predicted in total with the corresponding TDMs, Einstein A coefficients, and oscillator strengths. Partition functions for temperatures from 10 to 7500 K are also calculated for the eight isotopologues of CS in their ground electronic states. The line lists enlarge the spectroscopic transitions of CS to a large extent and can be used in detections of CS in astronomical environments of various temperatures.

This work was supported by the Shandong Province Natural Science Foundation (ZR2015AM009). The referee is greatly appreciated for incisive comments, which led to considerable strengthening of this paper.

ORCID iDs

Shilin Hou  <https://orcid.org/0000-0002-7873-9214>

References

- Ahrens, V., & Winnewisser, G. 1999, *ZNatA*, **54**, 131
Aoki, W., Tsuji, T., & Ohnaka, K. 1998, *A&A*, **340**, 222
Bernath, P. F. 2014, *RSPTA*, **372**, 20130087
Bernath, P. F. 2016, *Spectra of Atoms and Molecules* (3rd ed.; New York: Oxford Univ. Press)
Bogey, M., Demuynck, C., & Destombes, J. L. 1982, *JMoSp*, **95**, 35
Burkholder, J. B., Lovejoy, E., Hammer, P. D., et al. 1987, *JMoSp*, **124**, 450
Canaves, M., de Almeida, A., Boice, D., et al. 2007, *AdSpR*, **39**, 451
Carlson, T. A., Copley, J., Durici, N., et al. 1979, *CP*, **42**, 81
Coppens, P., & Drowart, J. 1995, *CPL*, **243**, 108
Cossart, D., Horani, M., & Rostas, J. 1977, *JMoSp*, **67**, 283
Coxon, J. A., & Hajigeorgiou, P. G. 1992, *CP*, **167**, 327
Crawford, F. H., & Shurcliff, W. A. 1934, *PhRv*, **45**, 860
Danilovich, T., Richards, A. M. S., Karakas, A. I., et al. 2019, *MNRAS*, **484**, 494
Destree, J. D., Snow, T. P., & Black, J. H. 2009, *ApJ*, **693**, 804
Donovan, R. J., Husain, D., & Stevenson, C. D. 1970, *Trans. Faraday Soc.*, **66**, 1
Dunning, T. H. 1989, *JChPh*, **90**, 1007
Edwards, J. L., & Ziurys, L. M. 2014, *ApJL*, **794**, L27
Fournier, J., Deson, J., Vermeil, C., et al. 1979, *JChPh*, **70**, 5703
Gdanitz, R. J., & Ahlrichs, R. 1988, *CPL*, **143**, 413
Hasegawa, T., Kaifu, N., Inatani, J., et al. 1984, *ApJ*, **283**, 117
Hayashi, M., Omodaka, T., Hasegawa, T., et al. 1985, *ApJ*, **288**, 170
Heays, A. N., Bosman, A. D., & van Dishoeck, E. F. 2017, *A&A*, **602**, A105
Heikkilä, A., Johansson, L. E. B., & Olofsson, H. 1999, *A&A*, **344**, 817
Herpin, F., Chavarría, L., van der Tak, F., et al. 2012, *A&A*, **542**, 76
Hou, S., & Bernath, P. F. 2017, *JQSRT*, **203**, 511
Hynes, A. J., & Brophy, J. H. 1979, *CPL*, **63**, 93
Indebetouw, R., Brogan, C., Chen, C. H. R., et al. 2013, *ApJ*, **774**, 73
Kawaguchi, K., & Deo, M. N. 2019, *JMoSp*, **362**, 96
Kendall, R. A., Dunning, T. H., & Harrison, R. J. 1992, *JChPh*, **96**, 6796
Kim, E., & Yamamoto, S. 2003, *JMoSp*, **219**, 296
Knowles, P. J., & Werner, H. J. 1985, *CPL*, **115**, 259
Knowles, P. J., & Werner, H. J. 1988, *CPL*, **145**, 514
LeRoy, R. J. 2017a, *JQSRT*, **186**, 179
LeRoy, R. J. 2017b, *JQSRT*, **186**, 167
LeRoy, R. J., & Huang, Y. 2002, *JMoSt*, **591**, 175
Li, C., Deng, L., Zhang, J., et al. 2013a, *JMoSp*, **284**, 29
Li, G., Gordon, I. E., LeRoy, R. J., et al. 2013c, *JQSRT*, **121**, 78
Li, R., Wei, C. L., Sun, Q. X., et al. 2013b, *JPCA*, **117**, 2373
Mahon, C. A., Stampanoni, A., Luque, J., et al. 1997, *JMoSp*, **183**, 18
Maxted, N., Burton, M., Braiding, C., et al. 2018, *MNRAS*, **474**, 662
McGuire, B. A. 2018, *ApJS*, **239**, 17
Medvedev, E. S., Meshkov, V. V., Stolyarov, A. V., et al. 2016, *JMoSp*, **330**, 36
Medvedev, E. S., Ushakov, V. G., Stolyarov, A. V., et al. 2017, *JChPh*, **147**, 164309
Mockler, R. C., & Bird, G. R. 1955, *PhRv*, **98**, 1837
Moreno, R., Marten, A., Matthews, H. E., et al. 2003, *P&SS*, **51**, 591
Müller, H. S. P., Schlöder, F., Stutzki, J., et al. 2005, *JMoSt*, **742**, 215
Ornellas, F. R. 1998, *CPL*, **296**, 25
Pattillo, R. J., Cieszewski, R., Stancil, P. C., et al. 2018, *ApJ*, **858**, 10
Paulose, G., Barton, E. J., Yurchenko, S. N., et al. 2015, *MNRAS*, **454**, 1931
Penzias, A. A., Solomon, P. M., Wilson, R. W., et al. 1971, *ApJL*, **168**, L53
Pickett, H. M., Poynter, R. L., Cohen, E. A., et al. 1998, *JQSRT*, **60**, 883
Pineiro, A. L., Tipping, R. H., & Chackerian, C. 1987, *JMoSp*, **125**, 91
Ram, R. S., Bernath, P. F., & Davis, S. P. 1995, *JMoSp*, **173**, 146
Riaz, B., Thi, W. F., & Caselli, P. 2019, *MNRAS*, **483**, 1139
Ridgway, S. T., Hall, D. N. B., & Carbon, D. F. 1977, *BAAS*, **9**, 636
Rubio, M., Paron, S., & Dubner, G. 2009, *A&A*, **505**, 177
Shi, D. H., Li, W. T., Zhang, X. N., et al. 2011, *JMoSp*, **266**, 27
Smith, W. H. 1969, *JQSRT*, **9**, 1191
Stark, G., Yoshino, K., & Smith, P. L. 1987, *JMoSp*, **124**, 420
Tenenbaum, E. D., Dodd, J. L., Milam, S. N., et al. 2010, *ApJS*, **190**, 348
Tennyson, J., Yurchenko, S. N., Al-Refaie, A. F., et al. 2016, *JMoSp*, **327**, 73
Todd, T. R. 1977, *JMoSp*, **66**, 162
Uehara, H., Horiai, K., & Sakamoto, Y. 2015, *JMoSp*, **313**, 19
Vidler, M., & Tennyson, J. 2000, *JChPh*, **113**, 9766
Watson, J. K. G. 1980, *JMoSp*, **80**, 411
Werner, H. J., & Knowles, P. J. 1985, *JChPh*, **82**, 5053

- Werner, H. J., & Knowles, P. J. 1988, *JChPh*, **89**, 5803
- Werner, H. J., & Knowles, P. J. 1990, *AcTC*, **78**, 175
- Werner, H. J., Knowles, P. J., Knizia, G., et al. 2012, *WIREs Comput. Mol. Sci.*, **2**, 242
- Werner, H. J., Knowles, P. J., Knizia, G., et al. 2015, MOLPRO (Version 2015.1), a Package of Ab Initio Programs, <http://www.molpro.net>
- Western, C. M. 2017, *JQSRT*, **186**, 221
- Winkel, R. J., Davis, S. P., Pecyner, R., et al. 1984, *CaJPh*, **62**, 1414
- Winnewisser, G., & Cook, R. L. 1968, *JMoSp*, **28**, 266
- Woodney, L. M., A'Hearn, M. F., McMullin, J., et al. 1997, *EM&P*, **78**, 69
- Woon, D. E., & Dunning, T. H. 1993, *JChPh*, **98**, 1358
- Ziurys, L. M., Milam, S. N., Apponi, A. J., et al. 2007, *Natur*, **447**, 1094